Korean J. Chem. Eng., **27**(2), 480-486 (2010)
DOI: 10.1007/s11814-010-0095-9

Suppression of carbon formation in steam reforming of methane by addition of Co into Ni/ZrO_2 catalysts

Dasika Harshini*,, Yongchai Kwon***, Jonghee Han*,†, Sung Pil Yoon*, Suk Woo Nam*, and Tae-Hoon Lim***

*Fuel Cell Research Center, Korea Institute of Science and Technology, Seoul 130-650, Korea
**School of Engineering, University of Science and Technology, Daejon 305-330, Korea
***Department of Chemical and Environmental Technology, Inha Technical College, 253, Yonghyun-dong, Nam-gu, Incheon 402-752, Korea
(*Received 23 June 2009 • accepted 14 September 2009*)

Abstract−We investigated the steam reforming of methane (SRM) over various NiCo bimetallic catalysts supported on ZrO_2 to determine whether the addition of Co on the Ni catalyst suppressed carbon formation. The effect of metal loading on SRM reaction was evaluated in a downflow tubular fixed-bed reactor under various steam-to-carbon (S/C) ratios and temperatures. For monitoring changes in the catalysts before and after the SRM reactions, several techniques (BET, XRD, TEM, and CHN analysis) were used. The effects of reaction temperature, gas hourly space velocity (GHSV), and molar S/C ratios were studied in detail over the various catalyst combinations. It was found that an Ni-to-Co ratio of 50 : 50 supported on ZrO_2 provided the best catalytic activity, along with an absence of coking, when operated at a temperature of 1,073 K, a GHSV of 24 L g^{-1} h^{-1}, and an S/C ratio of 3 : 1.

Key words: Methane, Steam Reforming, Bimetallic NiCo Alloy Catalysts

INTRODUCTION

The catalytic steam reforming of methane (SRM) is used worldwide as the main technology for the large-scale production of hydrogen [1-3]. Recently, this reaction has become more important as a means for the prior processing of fuel cell feedstock gas [4]. The metallic elements in group VIII of the periodic table are all essentially active catalysts for this reaction. The SRM reactions are outlined in reactions (1) and (2) [1-3]:

$$CH_4+H_2O\rightarrow 3H_2+CO\ (\Delta H=+206\ kJ\ mol^{-1}) \quad (1)$$

$$CO+H_2O\rightarrow CO_2+H_2\ (\Delta H=-41\ kJ\ mol^{-1}) \quad (2)$$

Ceramic-supported nickel catalysts are both favored and widely used in the industry because of their high activity, their relatively long life spans, and their significantly lower utilization costs, in comparison with the other precious metal-based catalysts [3,5-9]. Nevertheless, catalyst aging (deactivation) and subsequent formation of surface coke are major problems that make it difficult to use this metal on large scales [5-12]. Generally, when hydrocarbons are exposed to high temperatures, the formation of superficial carbon deposits often occurs through the formation of C-C and C=C bonds from the hydrocarbon chains on the exposed catalyst surfaces. Thus, during the production of synthesis gas from natural gas (NG), carbon deposits are often formed through decomposition of the methane feedstock (reaction (3)) or through the Boudouard reaction (4):

$$CH_4\rightarrow C+2H_2;\ (\Delta H^{o}_{298}=75\ kJ\ mol^{-1}) \quad (3)$$

$$2CO\rightarrow C+CO_2;\ (\Delta H^{o}_{298}=-172\ kJ\ mol^{-1}) \quad (4)$$

†To whom correspondence should be addressed.
E-mail: jhan@kist.re.kr

The coking problem is particularly severe for Ni-based catalysts. Although other tested metals, including Pt, Pd, Rh, and Ru, exhibit better resistance toward carbon deposition [13-15], they are prohibitively expensive. Because Ni is much cheaper, there is currently much research aimed at improving the stability and coking resistance of Ni-based catalysts.

It is proposed that during CH_4/CO_2 reforming, the coke species formed by decomposition of CH_4 on the metal has to be removed by the activated oxygen species derived from CO_2. Takanabeet al.. [16] and Ruckenstein et al. [17] showed that the Co catalysts tended to be deactivated by oxidation of the metal, implying that the oxygen species derived from CO_2 reacts more preferentially with Co than the coke species derived from CH_4. This proves that Co has stronger affinity towards oxygen species, which can suppress the carbon formation during reforming reactions.

The addition of Co to Ni catalyst suppresses coke formation by various reactions, including the partial oxidation of methane to synthesis gas [18,19], the steam reforming of propane and acetic acid [20-22], and the CO_2 reforming of methane [23,24]. There is relatively little data, however, related to the suppression of carbon formation after the addition of Co to Ni catalysts applied to the SRM reaction. Thus, our objective in this study was to combine the strong affinity of Co for oxygen species with the strong affinity of Ni for carbon species to suppress carbon formation and, thereby, increase the methane conversions and product yields of the SRM reaction. We investigated the behavior of these catalysts with respect to several factors: the Ni-to-Co ratio, the steam-to-carbon ratio (S/C ratio), the gas hourly space velocity (GHSV), and the reaction temperature.

EXPERIMENTAL

ZrO_2 powder, a support for the catalysts, was prepared using the

precipitation method, with zirconyl nitrate [$ZrO(NO_3)_2 \cdot 2H_2O$] as the precursor and aqueous ammonia solution as the hydrolyzing agent. In a typical experiment, aqueous ammonia solution was added to 0.1 M aqueous $ZrO(NO_3)_2 \cdot 2H_2O$ until the solution reached pH 9. The resulting precipitate was filtered off, washed thoroughly with water, dried at 373 K for 12 h in an oven, and finally calcined at 873 K for 4 h in a muffle furnace to obtain monoclinic ZrO_2.

Bimetallic NiCo catalysts featuring various Ni/Co ratios were prepared on the ZrO_2 supports through co-impregnation in an aqueous solution of their respective nitrates. The two metals were deposited at various compositions, but the loading amount was kept constant at 10 wt% with respect to the support. The prepared catalysts were then dried for 12 h and calcined at 873 K for 4 h in flowing air to remove the ligands from the Co and Ni precursors. For a ratio of Ni to Co of m:n, the samples are denoted as "NiCo(m:n)/S," where S is the support [25].

Elemental analysis of the samples was performed using inductively coupled plasma/atomic emission spectroscopy (ICP). X-ray diffraction (XRD) patterns were collected at room temperature using a Rigaku X-ray diffractometer (M18XHF-SRA, Mac Science, Japan) with Cu K-α1/30 kV/100 mA. The spectra were scanned in the 2θ range from 3 to 90° at a rate of 5° min^{-1} to examine the phase structures of the catalysts. Brunau, Emmett and Teller (BET) tests were performed to measure the specific surface areas of the mixed oxides through adsorption of N_2 using a Micrometrics ASAP 2000 apparatus. Carbon formation on the catalyst during tests of activity was measured through elemental analysis in an elemental analyzer EA1108 (model CHNS-0), using 2 mg of the sample in a tin capsule and a furnace temperature of 1,293 K. The morphologies and particle sizes of the catalysts were analyzed by a Technai G2 F20 transmission electron microscope (TEM).

The SRM was conducted under atmospheric pressure in a fixed-bed quartz reactor (inner and outer diameters: 8 and 9 mm, respectively). The temperature of the reactor was controlled by a temperature controller equipped with a thermocouple placed near the catalyst bed. Fresh catalyst (0.5 g) was reduced in a H_2 flow (30 mL/min, 100% H_2) at 973 K for 2 h. The catalyst was then flushed with N_2 for 30 min and then exposed to the reaction gases: a mixture of CH_4 (99.95% purity) and steam. The effects of the temperature, GHSV, and S/C ratio on the various NiCo catalysts were studied. An iced water trap was located at the reactor exit to remove the steam contained in the effluent gas. A portion of the dried effluent gas (containing H_2, CO, CH_4, and CO_2) was analyzed through online gas chromatography (Agilent micro GC 3000A) using molecular sieves, plot U columns, and a thermal conductivity detector (TCD). N_2 was used as a tie balance. The H_2 and CO yields were obtained from the CH_4 conversion. The CH_4 conversion and H_2, CO, and CO_2 yields are defined herein as follows [26]:

$$CH_4 \text{ Conversion } (\%) = \left(\frac{n\ CH_4\ in - n\ CH_4\ out}{n\ CH_4\ in}\right) \times 100$$

$$H_2 \text{ Yield} = \left(\frac{n\ H_2\ out}{n\ CH_4\ in}\right)$$

$$CO \text{ Yield} = \left(\frac{n\ CO\ out}{n\ CH_4\ in}\right)$$

$$CO_2 \text{ Yield} = \left(\frac{n\ CO_2\ out}{n\ CH_4\ in}\right)$$

where n is the number of moles

RESULTS AND DISCUSSION

1. Characterization of Catalysts Prior to SRM

Table 1 lists the BET surface areas of the calcined catalysts. The surface areas of the bimetallic catalysts supported on oxides decreased slightly after the impregnation process. This reduction in surface areas after metal loading might have been caused by the deposited metals plugging the small pores in the Ni catalyst.

Fig. 1 displays XRD patterns of the various NiCo/ZrO_2 catalysts. In Fig. 1(a), we observe that monoclinic ZrO_2 (JCPDS No. 830944) was formed, while the XRD patterns of the bimetallic NiCo peaks revealed alloy formation. To investigate the formation of the NiCo alloy more intensively, we investigated the (111) plane of the metallic peak over a narrow scanning range (2θ=44-45°). Fig. 1(b) reveals that the NiCo bimetallic peak shifted from Co (44.2°) to Ni (44.5°) upon decreasing the Co content, confirming the formation of the NiCo alloy [17]. Table 1 also lists the amounts of the loaded metals, as determined through ICP analysis and calculated from the XRD patterns. We conclude that the metal loadings matched the precursor metal contents well.

2. Effect of Reaction Temperature on SRM

Fig. 2 and Table 2 reveal the effect of the catalytic activities for the SRM reactions over the temperature range from 773 to 1,173 K. These tests were performed using the catalysts prepared at an S/C ratio of 3 and a GHSV of 24 L g^{-1} h^{-1}. Fig. 2 also shows the equilibrium CH_4 conversion with the reaction temperature at 1 atm. CH_4 conversion increases with the increasing temperature in this tem-

Table 1. BET surface area for all the oven dried NiCo samples, and elemental analysis (ICP-AES) data for all reduced NiCo samples

Catalyst	BET SA (m^2 g^{-1})	Metal contents in precursor solution (wt%)		Metal loading from XRD analysis (wt%)*		Metal loading from ICP analysis (wt%)	
		Ni	Co	Ni	Co	Ni	Co
NiCo(100 : 0)/ZrO_2	35	10	0	9.7	0	9.8	0
NiCo(75 : 25)/ZrO_2	33	6.6	3.3	6.8	3.1	7.1	2.7
NiCo(50 : 50)/ZrO_2	32	5	5	5.2	4.7	4.5	4.8
NiCo(25 : 75)/ZrO_2	34	3.3	6.6	3.2	6.5	3.1	6.8
NiCo(0 : 100)/ZrO_2	32	0	10	0	9.9	0	9.8

ZrO_2 surface area=55.3 m^2 g^{-1}

*Calculated from XRD patterns of the reduced catalysts

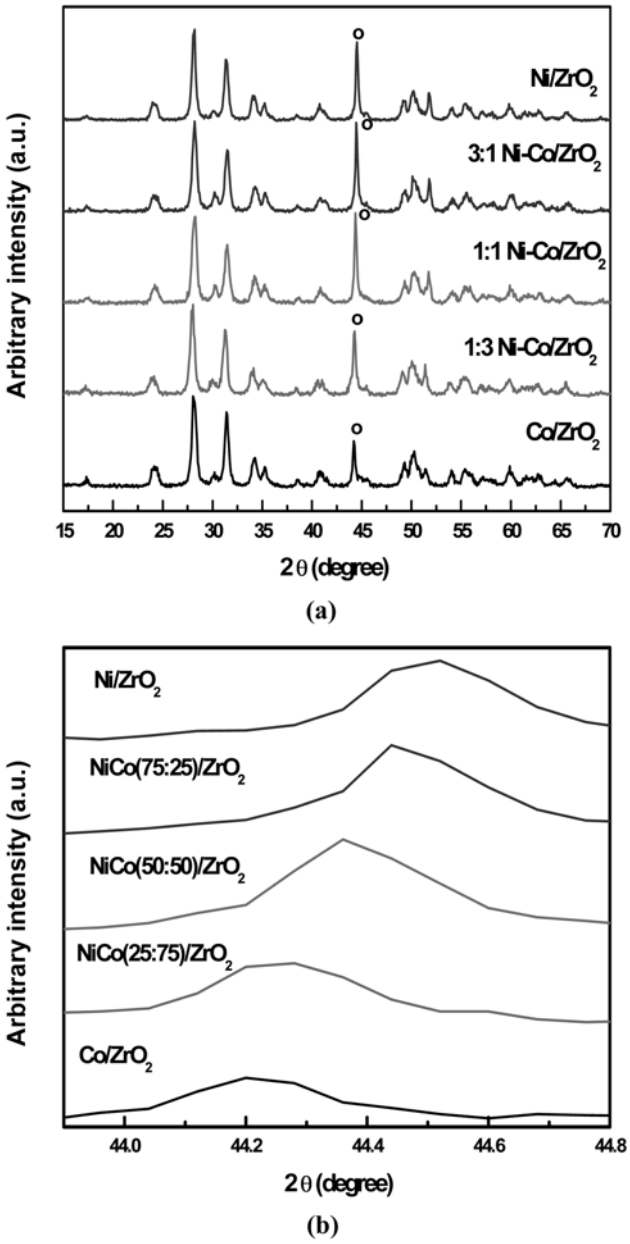

Fig. 1. (a) XRD patterns of all of the reduced catalysts supported on ZrO_2 (o=metal peak; Ni or Co). All the other peaks represent monoclinic ZrO_2. (b) XRD patterns of the samples in the narrow 2θ range from 44 to 45°.

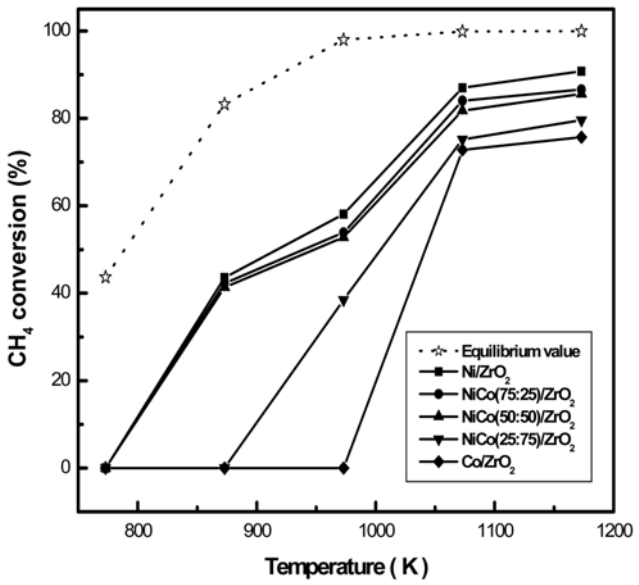

Fig. 2. Effect of temperature on the performance of all NiCo catalysts supported on ZrO_2 at S/C ratio: 3; GHSV: 24 L g^{-1} h^{-1}.

Table 2. Activities and yields to the products of all the ZrO_2-supported NiCo catalysts obtained after effect of temperature on SRM

Catalyst	Temperature (K)	H_2 yield	CO yield	CO_2 yield	H_2/CO
Ni/ZrO_2	773	0	0	0	0
	873	1.29	0.12	0.20	10.7
	973	1.80	0.22	0.30	8.0
	1073	2.76	0.76	0.10	3.6
	1173	3.20	0.91	0.08	3.4
$NiCo(75:25)/ZrO_2$	773	0	0	0	0
	873	1.28	0.12	0.22	10.2
	973	1.68	0.23	0.26	7.07
	1073	2.63	0.69	0.13	3.7
	1173	3.05	0.88	0.09	3.4
$NiCo(50:50)/ZrO_2$	773	0	0	0	0
	873	1.02	0.09	0.36	11.4
	973	1.62	0.17	0.26	9.2
	1073	2.56	0.70	0.13	3.6
	1173	2.99	0.87	0.06	3.4
$NiCo(25:75)/ZrO_2$	773	0	0	0	0
	873	0	0	0	0
	973	0.97	0.08	0.20	11.4
	1073	2.13	0.43	0.30	4.8
	1173	2.45	0.52	0.37	4.7
Co/ZrO_2	773	0	0	0	0
	873	0	0	0	0
	973	0	0	0	0
	1073	2.09	0.43	0.33	4.8
	1173	2.35	0.51	0.21	4.5

perature range. The theoretical thermodynamic equilibrium shows 99% CH_4 conversion at 1,073 K. In Fig. 2 we observe that the conversion of CH_4 increased upon increasing the reaction temperature or decreasing the Co content in the catalysts. As the temperature increased, the CO_2 yield decreased sharply; in contrast, the yields to H_2 and CO increased dramatically. This is because as the temperature increased the SRM reaction (1) became more prominent avoiding the WGS reaction (2), and also because at lower temperatures steam adsorbed on the surface of the catalyst could not be activated sufficiently [20]. At 773 K, we observed no activity for the catalysts for the SRM reactions. At 873 K, however, the Ni/ZrO_2, $NiCo\ (50:50)/ZrO_2$, and $NiCo\ (75:25)/ZrO_2$ catalysts (i.e., those containing low loadings of Co) began to mediate the methane conversion; the other two $NiCo\ (25:75)/ZrO_2$ and Co/ZrO_2 catalysts

(i.e., those containing high loadings of Co) did not mediate the methane conversion. Thus, when loading of Co in the catalysts was high, the reforming reaction of methane did not occur at lower temperatures [17]. The methane conversion rates did not vary significantly at temperatures above 1,073 K, irrespective of the composition of the bimetallic catalysts. Based on these results, we conclude that 1,073 K was the optimal reaction temperature for minimizing any undesirable effects (e.g., metal sintering) that might occur during high temperature processing of the bimetallic catalyst combinations; we employed it as the operating temperature for our subsequent analyses.

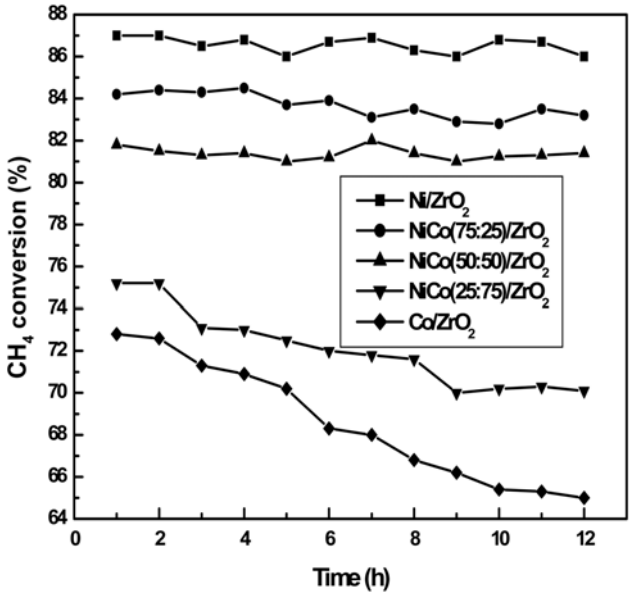

Fig. 3. Time-on-stream analysis of NiCo catalysts; temperature: 1073 K; S/C ratio: 3; GHSV: 24 L g^{-1} h^{-1}.

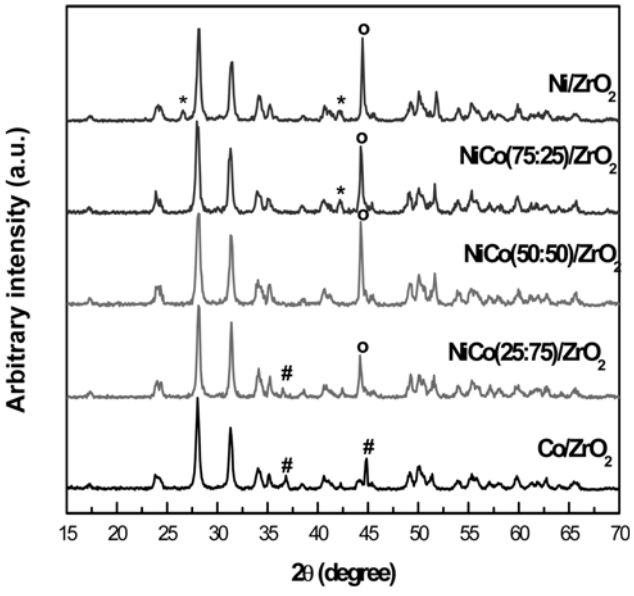

Fig. 4. XRD analyses of used catalysts; #=Co_3O_4; o=metal peak (Ni or Co); *=carbon formed on the catalysts.

Table 3. Carbon analysis data after time on stream analysis for 12 h

Catalyst	Carbon formed (wt%)[a]
Time-on-stream analysis (12 h)	
Ni/ZrO_2	1.6
$NiCo(75:25)/ZrO_2$	1.3
$NiCo(50:50)/ZrO_2$	0
$NiCo(25:75)/ZrO_2$	0
$Co//ZrO_2$	0

[a]Obtained from carbon analysis

3. Effect of Co Addition in the Catalysts on SRM

We performed "time on stream analyses" for all of our supported NiCo catalysts to determine whether the addition of Co to the Ni catalysts would effectively suppress carbon formation. The SRM reactions were conducted at 1,073 K for 12 h with an S/C ratio of 3 and a GHSV of 24 L g^{-1} h^{-1}. In Fig. 3, the "time on stream analyses" of the five NiCo catalysts, including the pure Ni and pure Co samples, reveal that the catalysts featuring lower Co contents [i.e., Ni/ZrO_2, $NiCo(75:25)/ZrO_2$, and $NiCo(50:50)/ZrO_2$] provided almost constant CH_4 conversions (87-86%, 84.2-83.2%, and 81.8-81.4%, respectively). Oxidation of the Co metal can be a cause for degradation in CH_4 conversion for catalysts with higher Co contents. XRD analysis (Fig. 4) revealed that carbon formation occurred during the reactions performed on the catalysts incorporating low contents of Co and oxidation of Co metal in catalysts containing higher contents of Co. Table 3 lists the amounts of carbon formed after the "time on stream analyses" performed for 12 h. It appears that deactivation of the methane conversions over the $NiCo(25:75)/ZrO_2$ and Co/ZrO_2 catalysts was due to oxidation of the Co metal to Co_3O_4 (Fig. 4). Thus, when the amount of Ni was small and the amount of Co was large, the oxidation reactions in the catalysts were limited; in addition, the carbon formation that occurred for the catalysts featuring high Ni contents could be controlled through the addition of an appropriate amount of Co to the catalyst. Therefore, there must be an Ni/Co ratio that provided the best SRM performance, i.e., without metal oxidation or carbon formation. Our results suggested that the $NiCo(50:50)/ZrO_2$ catalyst was the best bimetal composition in terms of its limiting of both metal oxidation and carbon formation. Therefore, we used this bimetal composition as a baseline catalyst for our subsequent experiments.

4. Effects of GHSV and S/C Ratio on $NiCo(50:50)/ZrO_2$

Fig. 5 displays the effect of the GHSV on the catalytic performance of the $NiCo(50:50)/ZrO_2$ catalyst. The tests were performed at 1,073 K with an S/C ratio of 3. Upon increasing the GHSV from 9.6 to 48 L g^{-1} h^{-1}, the CH_4 conversion decreased from 90 to 58.7% because of the decreased residence time of CH_4 on the surface of the catalyst. The GHSV also influenced the yields to the products: upon increasing the GHSV, the H_2 and CO yields decreased from 2.68 to 1.73 and from 0.64 to 0.38, respectively. We observed that 1.38 wt% carbon formation occurred on the catalyst spent at the GHSV of 9.6 L g^{-1} h^{-1}; in contrast, no carbon appeared on the catalyst spent at higher GHSVs. From all of these tests, we found that a GHSV of 24 L g^{-1} h^{-1} provided the optimal results: a CH_4 conversion of 81.8% with no carbon formation; therefore, we used these

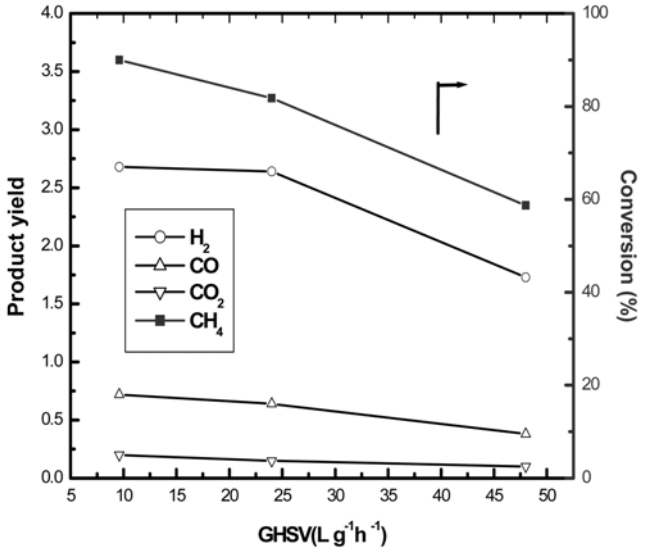

Fig. 5. Effect of the GHSV on the performance of the NiCo(50 : 50)/ZrO_2 catalyst.

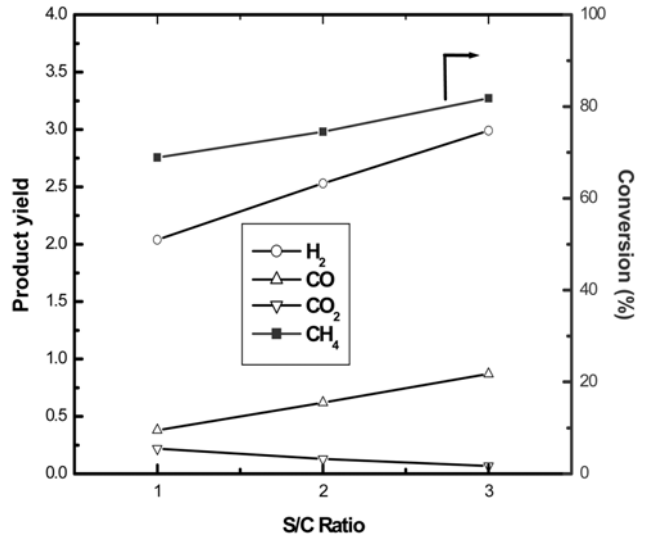

Fig. 6. Effect of the S/C ratio on the performance of the NiCo(50 : 50)/ZrO_2 catalyst.

conditions as a baseline for our subsequent reactions.

Fig. 6 reveals that the S/C ratio in the SRM reactions performed at 1,073 K and at a GHSV of 24 L g^{-1} h^{-1} had significant effects on both the CH_4 conversion and yields to the products. Upon increasing the S/C ratio from 1 to 3, the CH_4 conversion increased substantially from 68.9 to 81.8%, while the yields of the products H_2 and CO increased from 2.04 to 2.64 and from 0.38 to 0.72 respectively. A significant amount of CO_2 formed at the lower S/C ratios, but its yield decreased upon increasing the S/C ratio. This shows that as S/C ratio increased, the SRM reaction became more dominant, avoiding the formation of CO_2 at higher S/C ratios. The carbon content on the surface of the catalyst decreased significantly upon increasing the S/C ratio; formation of carbon and presence of higher amounts of CO_2 shows that Boudouard reaction was taking place at lower S/C ratios. When we performed the SRM reactions

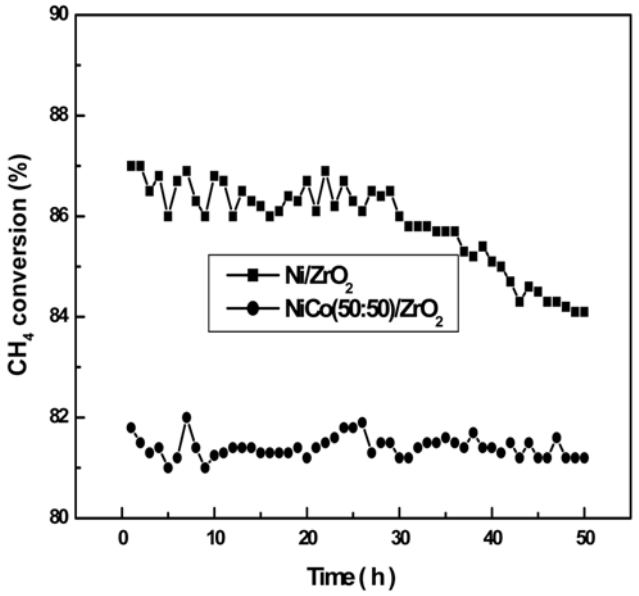

Fig. 7. Long-term stability tests of the Ni/ZrO_2 and NiCo(50 : 50)/ZrO_2 catalysts over 50 h.

Table 4. Crystallite sizes of all of the ZrO_2-supported NiCo catalysts as calculated from Scherrer equation

Catalyst	Metal crystallite size (nm)	
	Before reaction	After reaction
Ni/ZrO_2	39.98	48.72
NiCo(75:25)/ZrO_2	41.11	42.93
NiCo(50:50)/ZrO_2	38.67	41.11
NiCo(25:75)/ZrO_2	39.61	44.61
Co/ZrO_2	41.65	41.71

at S/C ratios of 1 and 2, we observed the formation of 1.45 and 1.3 wt% of carbon, respectively. In contrast, no carbon formation occurred in the SRM reaction performed at an S/C ratio of 3, which, gratifyingly, also provided higher methane conversions [27].

5. Long-term Stability Test

Fig. 7 displays the results of long-term stability tests for both the Ni/ZrO_2 and NiCo(50 : 50)/ZrO_2 catalysts, performed at an S/C ratio of 3 for a period of 50 h. For the Ni/ZrO_2 catalyst, we observed a decrease in the methane conversion from 87 to 84.1%, and about 8.3 wt% of carbon was formed, which led to a high pressure drop (from 20 to 73 cm H_2O) in the reactor during the SRM reaction. The carbon formation was confirmed through carbon analysis on the spent catalyst. This shows that the loss in catalytic activity is due to the carbon formation on the surface of catalyst, as the content of Ni in the catalyst is higher. We also noticed (Table 4) that there was a large increase in the Ni crystallite size-from 38.98 to 57.62 nm (calculated using the Scherrer equation [28])-which led to sintering of the catalyst. On the other hand, during the long-term stability test the NiCo(50 : 50)/ZrO_2 catalyst displayed a constant methane conversion of 81.8%, no carbon formation on the surface of the catalyst, a negligible pressure drop in the reactor, and an insignificant change in the crystallite size (from 38 to 43 nm). This shows that the presence of Co on the surface of the catalyst suppresses carbon

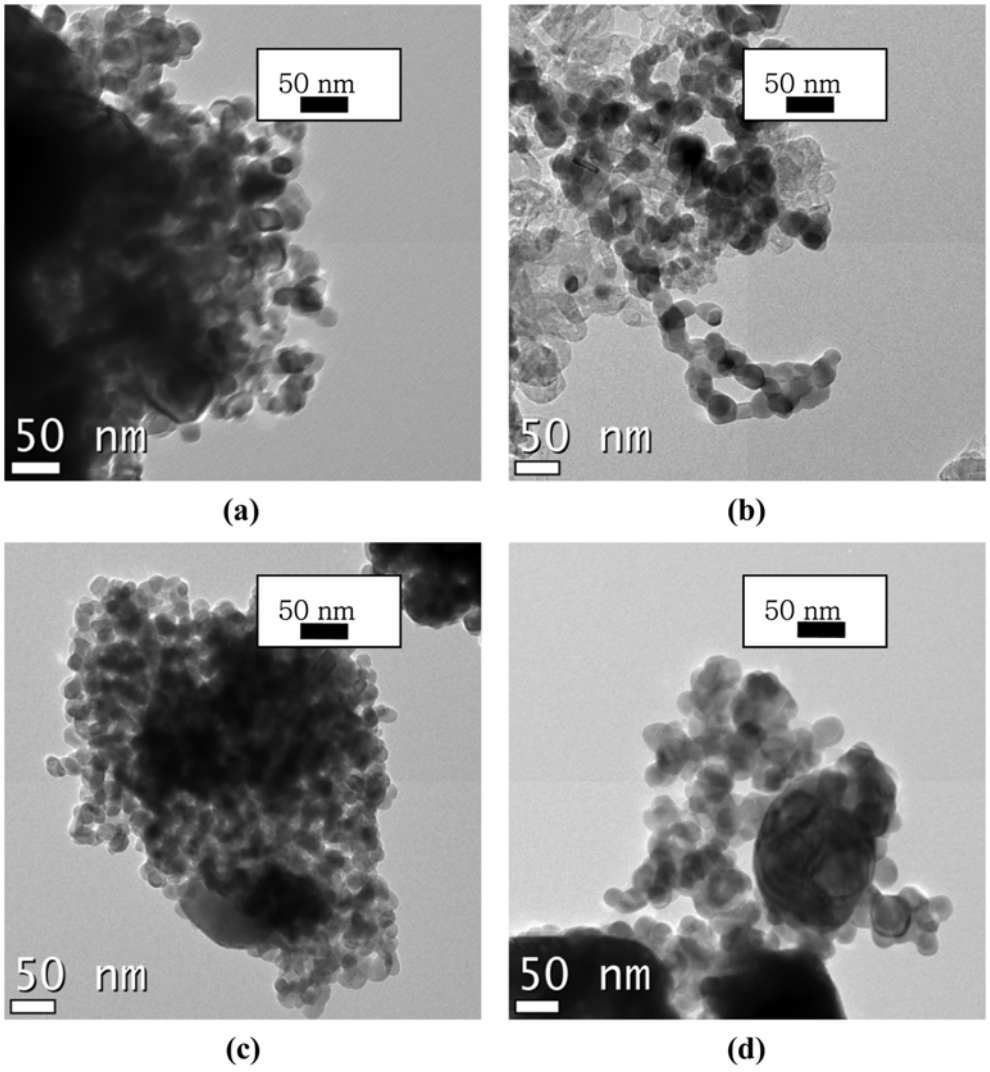

Fig. 8. TEM analysis of (a) the Ni/ZrO_2 catalyst before the SRM reaction, (b) the Ni/ZrO_2 catalyst after the SRM reaction for 50 h, (c) the $NiCo(50:50)/ZrO_2$ catalyst before the SRM reaction, and (d) the $NiCo(50:50)/ZrO_2$ catalyst after the SRM reaction for 50 h.

formation. TEM images of the Ni/ZrO_2 and $NiCo(50:50)/ZrO_2$ catalysts recorded before and after their SRM reactions (Fig. 8) reveal a large amount of carbon on the surface of the former catalyst, but no carbon on the latter. There was little change in the particle size for either catalyst. Thus, the long term stability tests confirmed that $NiCo(50:50)/ZrO_2$ was a better catalyst than Ni/ZrO_2 for the suppression of carbon formation during SRM reactions.

CONCLUSION

In terms of the ability to suppress carbon formation, Co-added Ni/ZrO_2 catalysts functioned better than unmodified Ni/ZrO_2 catalysts in SRM reactions. A Ni-to-Co ratio of 50 : 50 provided the best results: no carbon formation and superior catalytic activity. The reaction temperature, GHSV, and S/C ratio all had significant effects on the CH_4 conversions and product yields. Under the optimized conditions-a temperature of 1,073 K, a GHSV of 24 L g^{-1} h^{-1}, and an S/C ratio of 3-the $NiCo(50:50)/ZrO_2$ catalyst provided better catalytic activity during a long-term stability test performed over a period of 50 h, with no carbon formation, when compared with the performance of the corresponding Ni/ZrO_2 catalyst.

ACKNOWLEDGMENT

This study was supported financially by the Seoul R&D program.

REFERENCES

1. H. Kaihu and H. Ronald, *Chem. Eng. J.*, **82**, 311 (2001).
2. R. C. Vasant, B. Subhabrata and M. R. Amarjeet, *Appl. Catal. A*, **234**, 259 (2002).
3. M. Yasuyuki and N. Toshie, *Appl. Catal. A*, **258**, 107 (2004).
4. C. Song, *Catal. Today*, **77**, 17 (2002).
5. J. R. Rostrup-Nielsen, J. Sehested and J. K. Norskov, *Adv. Catal.*, **47**, 65 (2002).
6. H. S. Bengaard, J. K. Nørskov, J. Sehested, B. S. Clausen, L. P. Nielsen, A. M. Molenbroek and J. R. Rostrup-Nielsen, *J. Catal.*, **209**, 365 (2002).

7. J. R. Rostrup-Nielsen, J. R. Anderson and M. Boudart, *Catalysis Science and Technology*, Springer-Verlag, Berlin (1984).
8. D. L. Trimm, *Catal. Today*, **37**, 233 (1997).
9. J. R. Rostrup-Nielsen, *J. Catal.*, **33**, 184 (1974).
10. P. Forzatti and L. Lietti, *Catal. Today*, **52**, 165 (1999).
11. C. H. Bartholomew, *Appl. Catal. A*, **212**, 17 (2001).
12. D. L. Trimm, *Catal. Today*, **49**, 3 (1999).
13. S. Tang, J. Lin and K. L. Tan, *Catal. Lett.*, **59**, 129 (1999).
14. T. Wu, Q. Yan, F. Mao, Z. Niu, Q. Zhang, Z. Li and H. Wan, *Catal. Today*, **93**, 121 (2004).
15. S. Albertazzi, P. Arpentinier, F. Basile, P. Del Gallo, G. Fornasari, D. Gary and A. Vaccari, *Appl. Catal. A*, **247**, 1 (2004).
16. K. Takanabe, K. Nagaoka, K. Nariai and K. Aika, *J. Catal.*, **230**, 75 (2005).
17. E. Ruckenstein and H. Y. Wang, *J. Catal.*, **205**, 289 (2002).
18. V. R. Choudhary, A. M. Rajput, B. Prabhakar and A. S. Mamman, *Fuel*, **77**, 1803 (1998).
19. A. C. W. Koh, L. Chen, W. K. Leong, B. F. G. Johnson, T. Khimyak and J. Lin, *Int. J. Hydrogen Energy*, **32**, 725 (2007).
20. X. Hu and G. Lu, *J. Mol. Catal. A*, **261**, 43 (2007).
21. K. M. Hardiman, T. T. Ying, A. A. Adesina, E. M. Kennedy and B. Z. Dlugogorski, *Chem. Eng. J.*, **102**, 119 (2004).
22. K. M. Hardiman, C. H. Hsu, T. T. Ying and A. A. Adesina, *J. Mol. Catal. A*, **239**, 41 (2005).
23. K. Takanabe, K. Nagaoka, K. Narai and K. Aika, *J. Catal.*, **232**, 268 (2005).
24. V. R. Choudhary and A. S. Mamman, *J. Chem. Technol. Biotechnol.*, **73**, 345 (1998).
25. B. M. Reddy, G. K. Reddy, K. N. Rao, A. Khan and I. Ganesh, *J. Mol. Catal. A*, **265**, 276 (2006).
26. A. F. Lucredio and E. M. Assaf, *J. Power Sources*, **159**, 667 (2006).
27. H. Provendier, C. Petit and A. Kiennemann, *Chemistry*, **4**, 57 (2001).
28. H. P. Klug and L. E. Alexander, *X-ray diffraction procedures*, 2nd Ed., John Wiley & Sons Inc., U.S.A. (1974).